RSC Applied Polymers

ROYAL SOCIETY OF CHEMISTRY

PAPER

View Article Online
View Journal | View Issue

Cite this: *RSC Appl. Polym.*, 2024, **2**, 426

An organohydrogel with tunable fluorescence and shape-memory property for advanced anti-counterfeiting†

Yu Sun,[a,b] Hui Shang,[a,b] Xiaoxia Le *[a,b] and Tao Chen *[a,b,c]

Received 5th January 2024,
Accepted 10th February 2024

DOI: 10.1039/d4lp00003j

rsc.li/rscapplpolym

Counterfeiting is a significant threat in the intricate realm of global commerce, casting shadows over industries, economies, and unsuspecting consumers. Fluorescent anti-counterfeiting labels have been widely used in the past, but their level of security is still relatively inadequate. Therefore, the ongoing research is aimed at improving security through the encapsulation of information within predefined geometric structures. Herein, fluorescent organohydrogels with a hydrophilic polymer network of poly(*N*,*N*-dimethylacrylamide-acrylic acid) (P(DMA-AAc)), containing blue fluorescent monomers (PyMA), and a hydrophobic polymer network, polystearyl methylacrylate (PSMA), are fabricated by two-step interpenetrating polymerization. Upon treatment with Fe^{3+}, the blue fluorescence of organohydrogels is quenched owing to the intramolecular charge transfer (ICT) effect, which can be reinstated by adding H^+. Furthermore, coupled with the shape memory function induced by the crystallization of PSMA, the organohydrogels enable the concealment of encoded fluorescent information in specific three-dimensional shapes. This work presents innovative possibilities for designing and constructing advanced anti-counterfeiting systems.

1. Introduction

In a time of globalization and technological progress, counterfeiting has become a significant obstacle with far-reaching consequences for various industries, economies, and public welfare.[1–3] The consequences of counterfeiting go beyond economic considerations and include risks to public safety, damage to brand reputation, and the loss of consumer trust. Numerous materials and techniques have been developed to combat counterfeiting and have demonstrated effectiveness in reducing counterfeiting threats, including holograms,[4–6] watermarks,[7–9] Quick Response (QR) codes,[10–12] Radio-Frequency Identification (RFID),[13–15] and fluorescent patterns.[16–18] Among these technologies, fluorescent materials have risen as a novel frontier in the realm of anti-counterfeiting owing to their polychromatic attributes and wavelength-dependent characteristics, enhancing their utility in information security applications. However, the security of numerous fluorescent information encryption strategies remains deficient, as they can be decoded with singular ultraviolet light. Hence, advancing the substrate materials of fluorescent information in additional dimensions can further enhance information security.

Currently, efforts to address the issue of singular ultraviolet decoding of fluorescent anti-counterfeiting labels mainly focus on the construction of dual encryption systems, which can be achieved by controlling the fluorescence color for dynamic anti-counterfeiting and utilizing deformable substrate materials to conceal the loaded information. As the former is relatively difficult,[19–21] modulation of substrate materials with fluorescent patterns to realize dual encryption by adding the spatial dimension becomes an effective strategy. Intelligent gel materials exhibit outstanding stimulus-responsiveness, stability, and modifiability, and are easy to integrate with fluorescence emitters.[22,23] Simultaneously, their flexibility extends the possibilities of encryption in spatial and geometric shapes.[24] Yang *et al.*[25] prepared a gradient cross-linked fluorescent hydrogel responsive to temperature changes, serving as an information carrier readable under specific UV light irradiation, while self-deforming to reveal information as the temperature increases. Tang and coworkers[26] designed a bilayer hydrogel incorporating synergistic deformation and fluorescence color change through electrostatic interactions and dynamic covalent bonding, enabling ionoprinting of fluo-

[a]*Key Laboratory of Marine Materials and Related Technologies, Zhejiang Key Laboratory of Marine Materials and Protective Technologies, Ningbo Institute of Material Technology and Engineering, Chinese Academy of Sciences, Ningbo 315201, China. E-mail: lexiaoxia@nimte.ac.cn, tao.chen@nimte.ac.cn*
[b]*School of Chemical Sciences, University of Chinese Academy of Sciences, 19A Yuquan Road, Beijing 100049, China*
[c]*College of Material Chemistry and Chemical Engineering, Key Laboratory of Organosilicon Chemistry and Material Technology, Ministry of Education, Hangzhou Normal University, Hangzhou 311121, China*

†Electronic supplementary information (ESI) available. See DOI: https://doi.org/10.1039/d4lp00003j

rescent information. The encoded 2D bilayer hydrogel, capable of generating pre-designed 3D shapes to hide information, could only be read after the shapes were sequentially restored in the absence of background fluorescence. In our previous research,[27] we introduced a fluorescent hydrogel featuring simultaneous Fe^{3+}-responsive fluorescence quenching, borax-triggered shape memory, and inherent self-healing properties, concealing data loaded with Fe^{3+} ink within a complex 3D hydrogel origami structure to significantly enhance information security compared to its conventional 2D counterparts. However, the fluorescent hydrogel labels prepared in these studies were constrained by aqueous environments, posing a significant limitation to their further development.

This work synthesized the organohydrogels with both hydrophilic and hydrophobic networks, possessing reversible fluorescence switching and shape memory properties and exhibiting the capability to function in a desiccated state. The hydrophilic polymer network was synthesized through the copolymerization of *N*,*N*-dimethylacrylamide, acrylic acid, and 1-pyrenylmethyl acrylate (PyMA, blue fluorescence). Concurrently, the hydrophobic polymer network was derived from the polymerization of long-chain stearate methacrylate (SMA). Under the ultraviolet irradiation of 365 nm, PyMA emits blue fluorescence, which can be quenched by Fe^{3+} ions. This is due to the coordination of carboxylic acid groups on the hydrophilic polymer chains upon treatment with Fe^{3+} ions, which facilitates electron transfer between Fe^{3+} ions (electron acceptors) and PyMA fluorescent monomers (electron donors) *via* the ICT effect. Upon the additional introduction of H^+, the ICT process[28] between Fe^{3+} and PyMA would be terminated, thereby enabling the restoration of fluorescence color (Scheme 1a). Therefore, various fluorescent information can be loaded on the surface of the organohydrogels by ionoprinting and erased by treating with H^+. Additionally, the inherent low-temperature-induced crystallinity of PSMA endowed shape memory capabilities to the organohydrogels (Scheme 1b), establishing a foundation for the spatial dimension encryption of fluorescent labels. Subsequently, the organohydrogels with desired patterns were deformed into a specific configuration to complete the information encryption process. The hidden information could be decoded by successive steps of shape recovery and UV irradiation (Scheme 1c). Furthermore, the loaded information could be reversibly erased, allowing for multiple repetitions of the writing–encryption–decryption process. The prepared organohydrogels improved the information storage capacity and increased the security level of information encryption, which hold promising prospects in the advanced anti-counterfeiting field.

2. Experimental section

2.1 Materials

N,*N*-Dimethylacrylamide (DMA), *N*,*N*,*N*″,*N*′-tetramethylethylenediamine (TEMED), *N*,*N*″-methylene bis(acrylamide) (BIS), 2,2-diethoxyacetophenone (DEAP), ethylene dimethacrylate (EGDMA), 2-hydroxyethyl methacrylate (HEMA), 1-pyrenylbutyric acid and $FeCl_3{\cdot}6H_2O$ were purchased from Aladdin. Stearyl methylacrylate (SMA) was commercially provided by J&K Chemical Co., Ltd. Acrylic acid (AAc), HCl and DMSO were bought from Sinopharm Chemical Reagent Co., Ltd. The fluorescent monomer 1-pyrenylmethyl acrylate (PyMA) was synthesized according to our previous report. All reagents were used without any treatment or purification.

2.2 Preparation of the P(DMA-AAc-PyMA) hydrogel

First, 0.216 g AAc and 2.673 g DMA were dissolved in 2.01 mL deionized water. Second, 10 mg PyMA and 3 mg BIS were dispersed in 5 mL DMSO. After mixing the above two solutions, 70 mg APS and 46 μL TEMED were gradually added. After rapid shaking and mixing, the mixed solution was transferred to a homemade reaction cell. After polymerization in an oven at 60 °C for 5 h, the hydrogels were placed in a large amount of acetone to remove deionized water and DMSO.

2.3 Preparation of the P(DMA-AAc-PyMA)/PSMA organohydrogel

The naturally air-dried P(DMA-AAc-PyMA) hydrogels were immersed in oily precursor solutions consisting of 20 mL SMA, 10 mL ethanol, 100 μL DEAP, and 150 μL EGDMA and stored at 35 °C for 12 h in the dark. The fully soaked swollen hydrogels were then sandwiched between two pieces of quartz glass and polymerized under UV light for 2 h (365 nm, 50 W). Furthermore, the organohydrogels were soaked in ethanol in order to remove unreacted monomers and then placed in air to dry.

2.4 Multi-level encryption and decryption of information

The prepared P(DMA-AAc-PyMA)/PSMA organohydrogels were ionoprinted by bringing them into contact with filter paper soaked with Fe^{3+} (0.1 M, 15 min) to load the corresponding information. To hide the loaded information, special shapes were fixed onto the organohydrogels and stored in a 4 °C freezer for 10 minutes. The original shape was restored by heating the organohydrogels to 60 °C, and the information could be revealed under UV light. In addition, the organohydrogels stained with Fe^{3+} can be brought into contact with filter paper soaked with H^+ (0.1 M, 15 min) to erase the loaded information and further rewrite with Fe^{3+}.

2.5 Characterization

^1H NMR spectra were obtained from a Bruker Avance III 400 MHz spectrometer. Rheological characterization was carried out on a stress-controlled rheometer (TA-dhr2) with a parallel plate (25 mm) in frequency sweep mode (from 0.1 to 100 rad s^{-1}) at a constant shear strain of 1%. UV-Vis absorption and transmittance spectra were measured on a UV-Vis spectrophotometer (TU-1810, Purkinje General Instrument Co. Ltd). ATR-FTIR spectra were recorded on a Thermo Scientific Nicolet 6700 FT-IR spectrometer. Raman spectra were recorded on a confocal micro-Raman spectrometer (Renishaw inVia Reflex, Renishaw Instrument Co. Ltd). The digital photos of the hydrogels were taken under a UV lamp (ZF-5, 5 W, 365 nm). All fluorescence photographs were taken using the

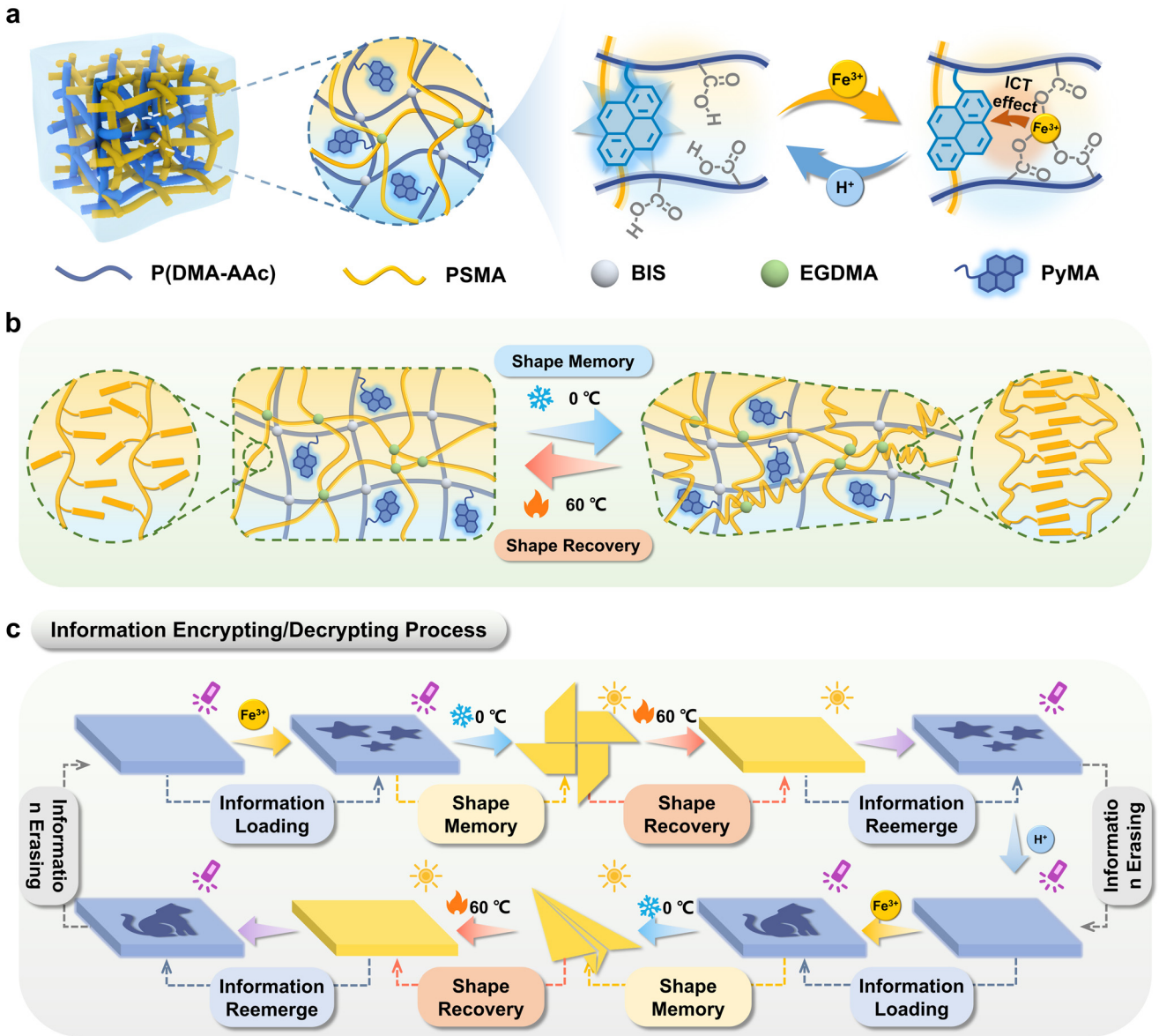

Scheme 1 Schematic illustration of the fluorescent organohydrogels P(DMA-AAc-PyMA)/PSMA for advanced encryption and decryption processes. (a) The fluorescent organohydrogels were composed of a hydrophilic polymer network and a hydrophobic network. Due to the ICT effect, Fe^{3+} leads to the quenching of the blue fluorescence, and H^+ reversibly restores the fluorescence colors. (b) Schematic diagram of the shape memory/recovery process of the organohydrogels P(DMA-AAc-PyMA)/PSMA. (c) Schematic diagram of the process of information encoding, encryption, and decryption.

same UV lamp. Fluorescence intensity was recorded with a HPRIBA FL3-111 fluorescence spectrometer. The excitation wavelength was 365 nm. SEM images were taken using a scanning electron microscope (S-4800, Hitachi).

3. Results and discussion

3.1 Fabrication of the P(DMA-AAc-PyMA)/PSMA organohydrogel

The synthesis of the fluorescent monomer (PyMA) involved the condensation of HEMA and 1-pyrenylbutyric acid (Fig. S1†), building upon established methodologies from previous work.[29] The ^{1}H NMR spectrum demonstrated the synthesis of the target fluorescent monomer, PyMA (Fig. S2†). The fluorescent organohydrogels were prepared by a two-step interpenetrating method (Fig. S3†). Specifically, the hydrogels, P(DMA-AAc-PyMA), were formed through copolymerization of the fluorescent PyMA monomer with acrylic acid (AAc) and *N*,*N*-dimethylacrylamide (DMA) in a mixed solvent system of water and dimethyl sulfoxide (DMSO), employing a free radical polymerization process with *N*,*N*″-methylene bis(acrylamide) (BIS) as the crosslinker, ammonium persulfate (APS) as the initiator, and *N*,*N*,*N*″,*N*′-tetramethylenediamine (TEMED) as

the accelerator. Furthermore, acetone immersion was employed to remove excess water and DMSO. Following natural air-drying, the dried hydrogels were thoroughly immersed in an oil gel precursor solution with SMA as the monomer, ethylene dimethacrylate (EGDMA) as the crosslinker, and 2,2-diethoxyacetophenone (DEAP) as the photosensitizer. Subsequently, the hydrogels saturated with the precursor were subjected to polymerization under UV irradiation to obtain the hydrophobic polymer network, resulting in the formation of the organohydrogels (Fig. 1a). The P(DMA-AAc-PyMA)/PSMA organohydrogels for follow-up research were achieved by purging unreacted monomers with ethanol and subsequently air-drying at room temperature. Additionally, to fully coordinate the carboxyl group of acrylic acid, the P(DMA-AAc-PyMA)/PSMA organohydrogel samples for the subsequent characterization were soaked in $FeCl_3$ solution (0.1 M) for 24 hours and naturally air-dried at room temperature.

3.2 Characterization of the P(DMA-AAc-PyMA)/PSMA organohydrogel

Compared to the hydrophilic P(DMA-AAc-PyMA) hydrogels (d = 22.13 ± 3.14 μm), the size of the porous structure of the P(DMA-AAc-PyMA)/PSMA organohydrogels showed an order of magnitude decrease (d = 0.61 ± 0.11 μm) as observed through a scanning electron microscope (SEM). Furthermore, the porous structure of the organohydrogels treated with Fe^{3+} immersion became denser (d = 0.14 ± 0.03 μm) (Fig. 1b–d and Fig. S4†) due to the coordination interaction between AAc and Fe^{3+}, leading to an increase in the crosslinking density and a decrease in pore size. The progressive densification of the porous structure from hydrogels to organohydrogels was further verified by a stepwise increase in the dynamic mechanical properties of energy storage modulus (G') and loss modulus (G'') (Fig. 1e). When a second layer of the hydro-

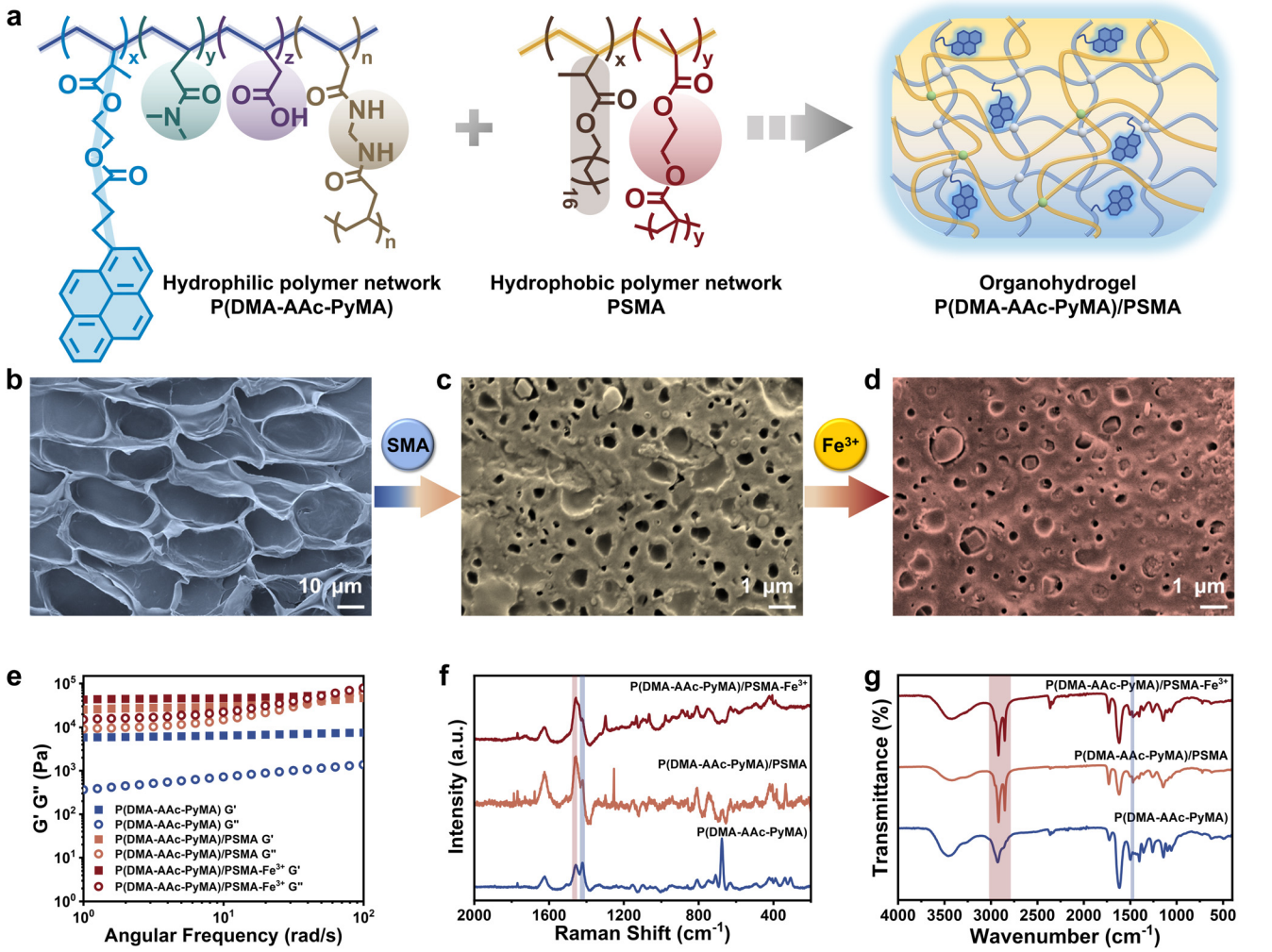

Fig. 1 Characterization of P(DMA-AAc-PyMA) hydrogels and P(DMA-AAc-PyMA)/PSMA organohydrogels before and after treatment with Fe^{3+}. (a) Schematic illustration of the internal molecular composition of the fluorescent organohydrogels. SEM images of (b) the P(DMA-AAc-PyMA) hydrogels and P(DMA-AAc-PyMA)/PSMA organohydrogels (c) before and (d) after treatment with Fe^{3+}. (e) Storage modulus (G') and loss modulus (G''), (f) Raman spectra and (g) FT-IR spectra of P(DMA-AAc-PyMA) hydrogels and P(DMA-AAc-PyMA)/PSMA organohydrogels before and after treatment with Fe^{3+}.

phobic polymer network was introduced, both G' and G'' of the organohydrogels were enhanced by orders of magnitude, compared to those of P(DMA-AAc-PyMA) hydrogels. It was also observed that both G' and G'' were slightly increased when the organohydrogels were treated with Fe^{3+}. The gradual reduction in transparency observed in both hydrophilic P(DMA-AAc-PyMA) hydrogels and P(DMA-AAc-PyMA)/PSMA organohydrogels before and after Fe^{3+} treatment (Fig. S5†) also served as evidence for densification.

To further validate the changes in the chemical composition of P(DMA-AAc-PyMA) hydrogels and P(DMA-AAc-PyMA)/PSMA organohydrogels with or without Fe^{3+} treatment, the Raman spectra were measured and analyzed (Fig. 1f). The presence of a distinct single peak at 1455.06 cm^{-1} suggested the carboxyl bonding composition of ester molecules, proving that the PSMA hydrophobic network was introduced into the hydrogel's molecular network. Following Fe^{3+} treatment, the disappearance of the peak at 1418.79 cm^{-1} (associated with C–O stretching and –OH deformation) was a result of the coordination between Fe^{3+} and the –COOH groups. Similarly, P(DMA-AAc-PyMA) hydrogels and P(DMA-AAc-PyMA)/PSMA organohydrogels with or without Fe^{3+} treatment were analyzed by attenuated total reflection Fourier transform infrared spectroscopy (ATR-FTIR). As shown in Fig. 1g, all samples showed an absorption peak at 1731.76 cm^{-1}, caused by the presence of C═O groups, and a characteristic peak at 2931.27 cm^{-1} generated by the antisymmetric stretching vibration of $-CH_2-$. However, the intensity of this peak is significantly higher in the organohydrogels due to the increase in C═O groups after the introduction of the PSMA polymer chain. At the same time, a new absorption peak appeared at 2850.27 cm^{-1}, indicating an increase in the introduction of $-CH_2-$, which indirectly proved the introduction of the hydrophobic polymer network of PSMA into organohydrogels. The elimination of the –OH bending peak at 1463.70 cm^{-1} subsequent to Fe^{3+} treatment underscored the coordination of Fe^{3+} with –COOH groups.

3.3 Reversible fluorescence switching process of the prepared organohydrogel

Due to the copolymerization of PyMA on hydrophilic polymer network chains, the organohydrogels emitted blue fluorescence under 365 nm. The initial P(DMA-AAc-PyMA)/PSMA organohydrogels exhibited blue fluorescence. However, upon treatment with strongly oxidative Fe^{3+} ions, coordination occurred between Fe^{3+} ions and carboxylic acid groups on the hydrophilic polymer chains (Fig. 2a), where Fe^{3+} ions became excellent electron acceptors due to their electron-deficient nature, leading to ICT between Fe^{3+} and fluorescence monomers PyMA (electron donors). This ICT phenomenon resulted in the rapid quenching of fluorescence from the PyMA as depicted in Fig. S6.† As shown in Fig. 2b, the photoluminescence (PL) mapping spectrum demonstrated the singular blue-emitting center of P(DMA-AAc-PyMA)/PSMA organohydrogels. Comparatively, Fe^{3+} treatment led to the disappearance of the blue emission center.

Furthermore, the degree of fluorescence quenching of the organohydrogels was also affected by the concentration of Fe^{3+} in solution as well as the soaking time. As shown in the fluorescence spectra of P(DMA-AAc-PyMA)/PSMA organohydrogels (Fig. 2c), the fluorescence intensity at 380 nm decreased with increasing time (0 to 30 min) of immersion in Fe^{3+} solution (0.1 M). With increasing immersion duration, there was not only a noticeable quenching of the fluorescence intensity but also a transformation of the organohydrogels. The organohydrogels displayed anisotropic swelling as the soaking time of one side of the organohydrogels in Fe^{3+} solution went from 0 min to 10 min (Fig. S7†), which is derived from chelation of Fe^{3+} within AAc, resulting in temporary cross-linking, and diminished the extent of swelling on one side. Relatively, when the immersion time was kept at 1 min, there was distinct weakening in the blue fluorescence with increasing Fe^{3+} content in the solution (0–125 mmol L^{-1}) (Fig. 2d). Coordinates of the organohydrogels without Fe^{3+} treatment was (0.1639, 0.1416) in the Commission Internationale de L′ Eclairage (CIE), but the organohydrogels with Fe^{3+} treatment did not exhibit them (Fig. 2e). It is important to emphasize that the organohydrogels displayed excellent cycling stability through the ICT effect of Fe^{3+} and the uncoordinated action of H^+, as seen in the fluorescence spectra (Fig. 2f). In light of the aforementioned remarkable reversible fluorescence quenching characteristics inherent in the organohydrogels, a sequential process encompassing information inscription, obliteration, and reinscription was achieved. A pattern of quenched fluorescence can be formed on the surface of an otherwise blue fluorescent organohydrogel by Fe^{3+} ion ionoprinting, and immediately thereafter, the introduction of H^+ ions can cause the quenched portion of the fluorescence to reappear. Notably, H^+ ions can be localized and brought into contact with the pattern of fluorescence quenching to achieve local recovery of local fluorescence. As illustrated in Fig. 2g, the initial introduction of the "raining" pattern was accomplished through Fe^{3+} (0.1 M, 15 min) ionoprinting. Subsequently, the "water drop" motif underwent erasure upon treatment with H^+ (0.1 M, 15 min), and in a subsequent step, the "lightning" pattern was re-ionoprinted and loaded once more through Fe^{3+} application.

3.4 Advanced encryption and decryption based on the P(DMA-AAc-PyMA)/PSMA organohydrogel

The constitution of organohydrogels involved a hydrophobic PSMA polymer network, which exhibits the capability to form microcrystalline domains under defined temperature conditions (Fig. S8†).[30] This inherent attribute imparted a shape memory function to the organohydrogels, enabling them to fold at high temperature (60 °C) and maintain a specific configuration at low temperature (0 °C) and subsequently recover the original shape when exposed to high temperatures again. Consequently, the integration of the reversible fluorescence switching phenomenon and shape memory characteristics in organohydrogels presented innovative avenues for implementing advanced information encryption and decryption strategies.

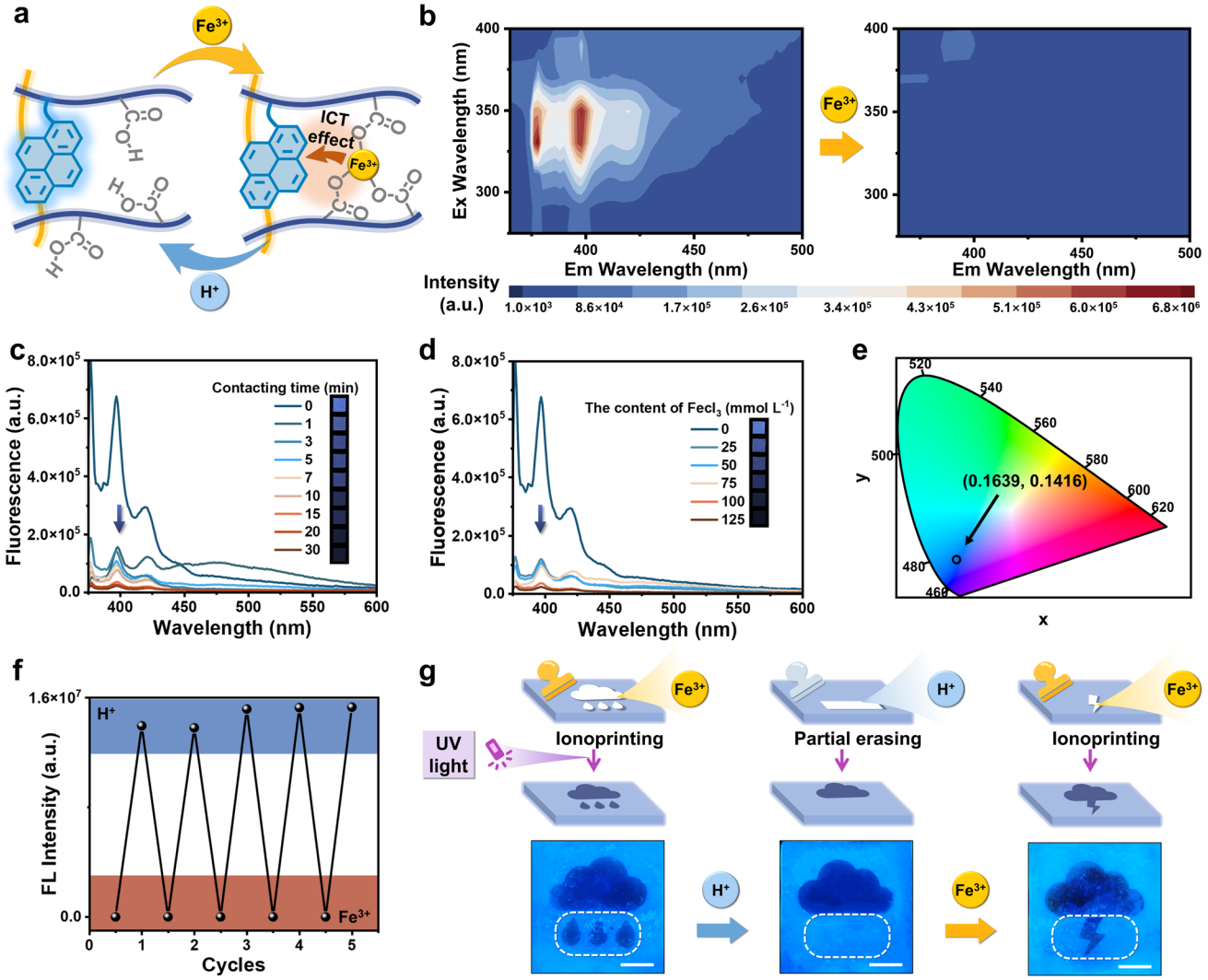

Fig. 2 Reversible fluorescence switching process. (a) Schematic illustration of the reversible fluorescence switching mechanism. Due to the ICT effect, fluorescence was quenched when adding Fe^{3+}, and subsequent treatment with H^+ led to the restoration of fluorescence. (b) PL mapping spectra of P(DMA-AAc-PyMA)/PSMA organohydrogels before and after Fe^{3+} (0.1 M) treatment (24 h). (c) Fluorescence spectra of the organohydrogels after various times of Fe^{3+} (0.1 M) treatment. (d) Fluorescence spectra of the organohydrogels immersed in solutions (1 min) containing different Fe^{3+} contents. (e) The fluorescence color of P(DMA-AAc-PyMA)/PSMA organohydrogels under 365 nm UV irradiation on the CIE (1931) chromaticity diagram. (f) The cyclic changes in the fluorescence intensity of organohydrogels following successive treatments with Fe^{3+} (0.1 M, 24 h) and H^+ (0.1 M, 24 h). (g) Schematic illustration and digital photos of the reversible fluorescence switching patterns were generated through the application of ionoprinting methodologies (scale bar: 1 cm).

As depicted in Fig. 3a, information encoding within the organohydrogels was initiated through the utilization of Fe^{3+} (0.1 M, 15 min) ionoprinting, and its reversible erasure was facilitated by the introduction of H^+ (0.1 M, 15 min). Additionally, the written information underwent concealment *via* a shape memory process at lower temperatures (0 °C). The revelation of this information was contingent upon the restoration of the original shape at high temperatures (60 °C), permitting decryption when the organohydrogels were subjected to UV light at a wavelength of 365 nm. To exemplify the proof-of-concept for advanced encryption and decryption, organohydrogels with a precisely rendered Quick Response Code (QR I) can undergo encryption by fixing the shape of the pinwheel at 0 °C (Fig. 3b). Following a 15-minute exposure in an oven (60 °C), the organohydrogel reverted to a flat shape. Illumination under UV light (365 nm) enabled the reacquisition of QR I information, such as "UCAS", accessible through smartphone scanning. The original information was erased through H^+ processing, thereby preparing the organohydrogels for the introduction of novel information. Subsequent encryption involved the concealment of "wrong information" within the shape of a butterfly, allowing for decryption and erasure under analogous conditions. Furthermore, QR II, coded as "NIMTE", was hidden within the geometric configuration of an airplane, and the information achieved encryption and decryption cycles facilitated by the shape memory and recovery process.

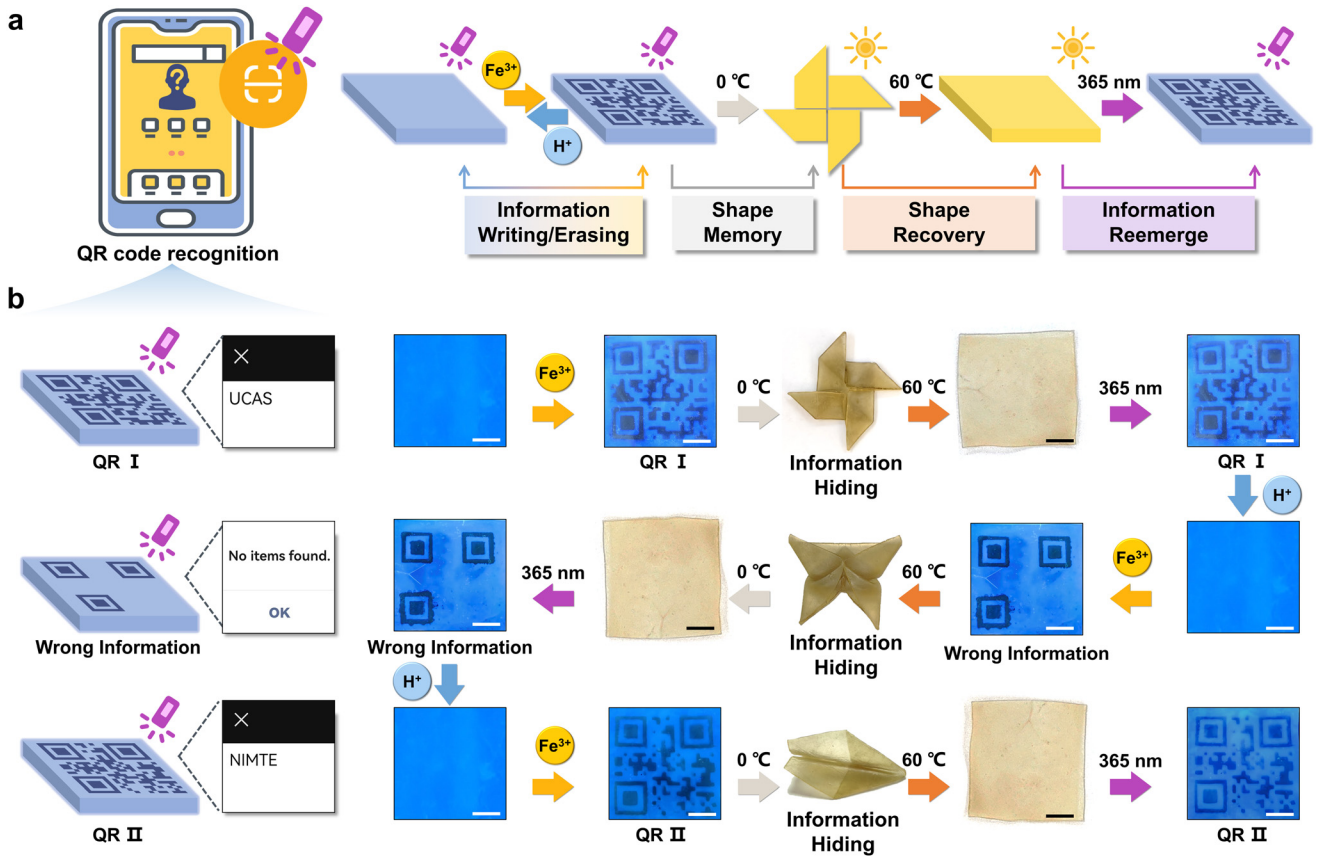

Fig. 3 Information encoding, encryption, and decryption processes based on the fluorescent organohydrogels with reversible fluorescence switching changes and shape memory properties. (a) Schematic illustration of information encoding, encryption, and decryption processes. (b) QR codes are precisely ionoprinted onto the organohydrogels in the presence of Fe^{3+}, and then the encoded information is further encrypted by a shape memory process. The hidden information could be obtained again under 365 nm UV light after shape recovery. H^+ treatment could erase the ionoprinted information for recoding new patterns on the organohydrogel (scale bar: 1 cm).

4. Conclusions

In this study, we reported an organohydrogel featuring dual hydrophilic and hydrophobic polymer networks, with the incorporation of the fluorescent monomers PyMA into the hydrophilic network. Hydroxy groups attached on the polymeric chains can coordinate with strongly oxidizing Fe^{3+}, inducing the intramolecular charge transfer phenomenon which results in the fluorescence quenching of the organohydrogel. This quenching phenomenon can further be eliminated through treatment with H^+. Additionally, the inherent crystalline properties of the hydrophobic polymer network contributed to the shape memory characteristics of the organohydrogel. The integration of reversible fluorescence switching with shape memory behavior facilitated advanced information encryption and decryption within the organohydrogels. In conclusion, our investigation proposes a novel approach for the design and fabrication of intelligent materials capable of advanced information storage. This innovation holds promise for enhancing information security and exhibits broad applicability in the realm of anti-counterfeiting.

Author contributions

Yu Sun: conceptualization, methodology, investigation, visualization and writing (original draft); Hui Shang: conceptualization, investigation, validation and writing (review & editing); Xiaoxia Le: supervision and writing (review & editing); Tao Chen: supervision.

Conflicts of interest

There are no conflicts to declare.

Acknowledgements

This work was supported by the National Key R&D Program of China (2022YFB3204300), the National Natural Science Foundation of China (52103246), the Zhejiang Provincial Natural Science Foundation of China (LQ22E030015), the Natural Science Foundation of Ningbo (2023J408,

20221JCGY010301), the Ningbo International Cooperation Project (2023H019), and the Sino-German Mobility Program (M-0424).

References

1 R. Arppe and T. Sørensen, *Nat. Rev. Chem.*, 2017, **1**, 0031.
2 Y. Sun, X. Le, S. Zhou and T. Chen, *Adv. Mater.*, 2022, **34**, 2201262.
3 Y. Shen, X. Le, Y. Wu and T. Chen, *Chem. Soc. Rev.*, 2024, **53**, 606–623.
4 D. Wen, F. Yue, G. Li, G. Zheng, K. Chan, S. Chen, M. Chen, K. Li, P. Wong, K. Cheah, E. Pun, S. Zhang and X. Chen, *Nat. Commun.*, 2015, **6**, 8241.
5 X. Li, L. Chen, Y. Li, X. Zhang, M. Pu, Z. Zhao, X. Ma, Y. Wang, M. Hong and X. Luo, *Sci. Adv.*, 2016, **2**, e1601102.
6 K. Lim, H. Liu, Y. Liu and J. Yang, *Nat. Commun.*, 2019, **10**, 25.
7 I. Cox, J. Kilian, F. Leighton and T. Shamoon, *IEEE Trans. Image Process.*, 1997, **6**, 1673–1687.
8 F. Hartung and M. Kutter, *Proc. IEEE*, 1999, **87**, 1079–1107.
9 H. Hu, H. Zhong, C. Chen and Q. Chen, *J. Mater. Chem. C*, 2014, **2**, 3695.
10 S. Han, H. Bae, J. Kim, S. Shin, S. Choi, S. Lee, S. Kwon and W. Park, *Adv. Mater.*, 2012, **24**, 5924–5929.
11 M. You, M. Lin, S. Wang, X. Wang, G. Zhang, Y. Hong, Y. Dong, G. Jin and F. Xu, *Nanoscale*, 2016, **8**, 10096–10104.
12 M. Li, W. Yao, J. Liu, Q. Tian, L. Liu, J. Ding, Q. Xue, Q. Lu and W. Wu, *J. Mater. Chem. C*, 2017, **5**, 6512–6520.
13 R. Singh, E. Singh and H. Nalwa, *RSC Adv.*, 2017, **7**, 48597–48630.
14 Y. Duroc and S. Tedjini, *C. R. Phys.*, 2018, **19**, 64–71.
15 S. Terranova, F. Costa, G. Manara and S. Genovesi, *Sensors*, 2020, **20**, 4740.
16 T. Ma, T. Li, L. Zhou, X. Ma, J. Yin and X. Jiang, *Nat. Commun.*, 2020, **11**, 1811.
17 C. Zhu, T. Bai, H. Wang, J. Ling, F. Huang, W. Hong, Q. Zheng and Z. Wu, *Adv. Mater.*, 2021, **33**, 2102023.
18 Q. Wang, B. Lin, M. Chen, C. Zhao, H. Tian and D. Qu, *Nat. Commun.*, 2022, **13**, 4185.
19 L. Ding and X. Wang, *J. Am. Chem. Soc.*, 2020, **142**, 13558–13564.
20 Z. Li, X. Ji, H. Xie and B. Tang, *Adv. Mater.*, 2021, **33**, 2100021.
21 K. Zhang, X. Zhou, S. Li, L. Zhao, W. Hu, A. Cai, Y. Zeng, Q. Wang, M. Wu, G. Li, J. Liu, H. Ji, Y. Qin and L. Wu, *Adv. Mater.*, 2023, **35**, 2305472.
22 Q. Ge, Z. Chen, J. Cheng, B. Zhang, Y. Zhang, H. Li, X. He, C. Yuan, J. Liu, S. Magdassi and S. Qu, *Sci. Adv.*, 2021, **7**, eaba4261.
23 X. Le, H. Shang, H. Yan, J. Zhang, W. Lu, M. Liu, L. Wang, G. Lu, Q. Xue and T. Chen, *Angew. Chem., Int. Ed.*, 2021, **60**, 3640–3646.
24 B. Wu, H. Lu, X. Le, W. Lu, J. Zhang, P. Théato and T. Chen, *Chem. Sci.*, 2021, **12**, 6472–6487.
25 X. Zuo, S. Wang, Y. Zhou, C. Wu, A. Huang, T. Wang and Y. Yang, *Chem. Eng. J.*, 2022, **447**, 137492.
26 C. Yang, H. Xiao, L. Tang, Z. Luo, Y. Luo, N. Zhou, E. Liang, G. Wang and J. Tang, *Mater. Horiz.*, 2023, **10**, 2496–2505.
27 Y. Zhang, X. Le, Y. Jian, W. Lu, J. Zhang and T. Chen, *Adv. Funct. Mater.*, 2019, **29**, 1905514.
28 S. Panja, N. Dwivedi and S. Saha, *RSC Adv.*, 2016, **6**, 105786–105794.
29 X. Le, W. Lu, J. He, M. Serpe, J. Zhang and T. Chen, *Sci. China Mater.*, 2019, **62**, 831–839.
30 H. Shang, X. Le, Y. Sun, F. Shan, S. Wu, Y. Zheng, D. Li, D. Guo, Q. Liu and T. Chen, *Adv. Opt. Mater.*, 2022, **10**, 2200608.